J Solid State Electrochem (2014) 18:1415–1423
DOI 10.1007/s10008-013-2190-4

ORIGINAL PAPER

Crystal structure and high-temperature electrical conductivity of novel perovskite-related gallium and indium oxides

S. Ya. Istomin · E. V. Antipov · Yu. S. Fedotov · S. I. Bredikhin · N. V. Lyskov · S. Shafeie · G. Svensson · Y. Liu · Z. Shen

Received: 28 May 2013 / Revised: 11 July 2013 / Accepted: 14 July 2013 / Published online: 31 July 2013

Abstract Novel complex oxides $Sr_2Ga_{1+x}In_{1-x}O_5$, x=0.0–0.2 with brownmillerite-type structure were prepared in air at T=1,273 K, 24 h. Study of the crystal structure of $Sr_2Ga_{1.1}In_{0.9}O_5$ refined using X-ray powder diffraction data (S.G. *Icmm*, a=5.9694(1) Å, b=15.2091(3) Å, c=5.7122(1) Å, χ^2=2.48, $R_F{}^2$=0.0504, R_p=0.0458) revealed ordering of Ga^{3+} and In^{3+} cations over tetrahedral and octahedral positions, respectively. A partial replacement of Sr^{2+} by La^{3+} according to formula $Sr_{1-y}La_yGa_{0.5}In_{0.5}O_{2.5+y/2}$, leads to the formation of a cubic perovskite (a=4.0291(5) Å) for y=0.3. No ordering of oxygen vacancies or cations was observed in $Sr_{0.7}La_{0.3}Ga_{0.5}In_{0.5}O_{2.65}$ as revealed by electron diffraction study. The trace diffusion coefficient (D_T) of oxygen for cubic perovskite $Sr_{0.7}La_{0.3}Ga_{0.5}In_{0.5}O_{2.65}$ is in the range 2.0×10^{-9}–6.3×10^{-8} cm^2/s with activation energy 1.4(1)eV as determined by isotopic exchange depth profile technique using secondary ion mass spectrometry at 973–1,223 K. These values are close to those reported for Ca-doped ZrO_2. High-temperature electrical conductivity of $Sr_{0.7}La_{0.3}Ga_{0.5}In_{0.5}O_{2.65}$ studied by AC impedance was found to be nearly independent on oxygen partial pressure. Calculated values of activation energy at T<1,073 K for hole and oxide-ion conductivities are 0.96 and 1.10 eV, respectively.

S. Y. Istomin (✉) · E. V. Antipov
Department of Chemistry, Moscow State University, Leninskie Gory, Moscow 119991, Russia
e-mail: istomin@icr.chem.msu.ru

Y. S. Fedotov · S. I. Bredikhin
Institute of Solid State Physics RAS, Chernogolovka 142432, Russia

N. V. Lyskov
Institute of Problems of Chemical Physics RAS, Chernogolovka 142432, Russia

S. Shafeie · G. Svensson · Y. Liu · Z. Shen
Department of Materials and Environmental Chemistry, Stockholm University, Stockholm 10691, Sweden

Keywords Brownmillerites · Perovskites · Crystal structure · Oxygen diffusion · High-temperature conductivity · Thermal expansion

Introduction

One the modern trends in the development of solid oxide fuel cells (SOFC) is to decrease their operation temperature down to 823–1,023 K (intermediate-temperature SOFC or IT-SOFC) [1]. However, new highly efficient materials for the components of SOFC are needed for such low working temperatures. This specially concerns cathode and electrolyte materials. Some perovskite-related oxides with group 13 elements of the Periodic Table like gallium and indium exhibit high oxide-ion conductivity at moderate temperatures and are considered as promising electrolyte materials for IT-SOFC. Thus A- and B-site doped $LaGaO_3$ is known to exhibit high oxide-ion conductivity at 873–1,073 K with ionic transport number (t_O) close to 1. The highest values of σ=0.17 and 0.08 S/cm were achieved for $La_{0.8}Sr_{0.2}Ga_{0.83}Mg_{0.17}O_{2.815}$ (LSGM) at 1,073 and 973 K, respectively [2]. $Ba_2In_2O_5$ with brownmillerite-type structure exhibits a phase transition to disordered perovskite at 1,198 K after which its conductivity drastically increases [3]. This disordered perovskite structure can be stabilized by A-site substitutions. Such phases exhibit the highest oxide ion conductivity for the cubic perovskite $(Ba_{0.3}Sr_{0.2}La_{0.5})_2In_2O_{5.5}$ with σ=0.12 S/cm at 1,073 K [4] which was tested as an electrolyte material for solid oxide fuel cells [5]. Mixed gallium–indium phases like $Ba_2In_{2-x}Ga_xO_5$ were also studied, however, they do not exhibit superior oxide-ion conductivities [6] and x>0.2 compositions represent perovskite-related structures different from brownmillerite or ideal perovskite [6, 7].

The brownmillerite-type structure is one of the most common among oxygen-deficient perovskites with the stoichiometry

$A_2B_2O_5$. It contains layers of corner-shared octahedra separated by oxygen-deficient layers with tetrahedral chains (Fig. 1). Among barium-contained complex oxides of group 13 elements only $Ba_2In_2O_5$ crystallizes in the brownmillerite structure. Strontium gallate $Sr_2Ga_2O_5$ is unknown and $Sr_2In_2O_5$ with brownmillerite structure was prepared in the form of single-crystals from a melt of $SrO\text{-}In_2O_3$ at 2,273 K and cannot be counted as a thermodynamically stable phase [8]. Recently, some of us reported on the formation of three novel phases Sr_2GaScO_5, $Sr_{10}Ga_6Sc_4O_{25}$, and $SrGa_{0.75}Sc_{0.25}O_{2.5}$ having, depending on Ga/Sc ratio, different perovskite-related structures [9]. One of these compounds Sr_2GaScO_5 represents a rare example of compounds with the brownmillerite structure where full ordering of cations over tetrahedral and octahedral positions takes place exclusively due to the size factor. Thus, Ga^{3+} cations (rGa^{3+}=0.47 Å, coordination number (CN)=4 and rGa^{3+}=0.62 Å, CN=6 [10]) occupy the tetrahedral sites in the structure, while large Sc^{3+} cations (rSc^{3+}=0.747 Å, CN=6 [10]) are located in octahedral positions. Taking into account that the ionic radius of In^{3+} (rIn^{3+}=0.8 Å, CN=6 [10]) in octahedral coordination is in the same size range as Sc^{3+}, one can assume the existence of brownmillerite-like Sr_2GaInO_5.

In the present work, we report on the synthesis and crystal structure study of novel oxide $Sr_2Ga_{1+x}In_{1-x}O_5$ with ordering of In^{3+} and Ga^{3+} cations on the octahedral and tetrahedral sites of the brownmillerite structure. Partial substitution of Sr^{2+} by La^{3+} according to the formula $Sr_{1-y}La_yGa_{0.5}In_{0.5}O_{2.5+y/2}$ leads to the formation of a cubic perovskite phase for y=0.3. High-temperature electrical conductivity of this compound at various oxygen partial pressures was studied. Oxygen tracer diffusion in $Sr_{0.7}La_{0.3}Ga_{0.5}In_{0.5}O_{2.65}$ was examined with the help of isotopic exchange depth profile (IEDP) technique using secondary ion mass spectrometry (SIMS).

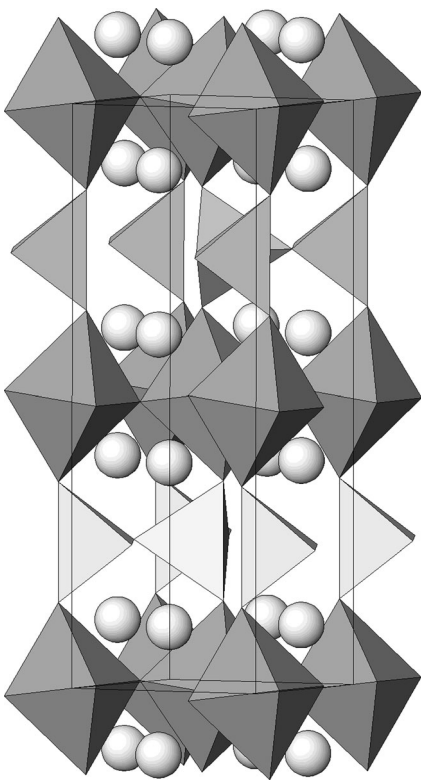

Fig. 1 The crystal structure of brownmillerite ($Ca_2(Fe,Al)_2O_5$)

Experimental

Samples of $Sr_2Ga_{1+x}In_{1-x}O_5$, x=0.0–0.2, Δx=0.05 and $Sr_{1-y}La_yGa_{0.5}In_{0.5}O_{2.5+y/2}$, y=0.1–0.5, Δy=0.1 were prepared from stoichiometric amounts of $SrCO_3$, Ga_2O_3, In_2O_3, and La_2O_3 preliminary annealed at 1,273 K, 24 h. Final heat treatment was performed in air at 1,473 K, 96 h with one intermediate regrinding after 48 h.

The phase purity of the compounds was checked by X-ray powder diffraction (XRPD) recorded in Huber G670 Guinier diffractometer ($CuK_{\alpha 1}$ radiation, image foil detector). The crystal structure of $Sr_2Ga_{1.1}In_{0.9}O_5$ was refined by Rietveld method using GSAS program package [11].

Electron diffraction (ED) patterns were recorded with a JEOL JEM2000FX TEM with a LaB_6 filament, equipped with a double tilt sample holder ±~45°, operating at 200 kV. The sample was fixed on a copper grid with holey carbon by dipping the grid through an ethanol suspension of the sample.

Dense ceramic samples of $Sr_{0.7}La_{0.3}Ga_{0.5}In_{0.5}O_{2.65}$ for the SIMS and AC impedance studies were prepared by spark plasma sintering (SPS). Approximately, 2.0–2.4 g of $Sr_{0.7}La_{0.3}Ga_{0.5}In_{0.5}O_{2.65}$ powders were filled into a graphite die with an inner diameter of 12 mm. The temperature was measured with an optical pyrometer focused on the surface of the graphite die and automatically regulated from 873 to 1,523 K or 1,573 K at a heating rate of 100 K/min. The temperature of 873 K was reached within 3 min via a preset heating program. The holding time was set to 5 min at the final sintering temperature. A constant uniaxial pressure of 75 MPa was applied during the whole sintering period. After sintering, a surface layer (about 0.5 mm) of the ceramic sample was removed by polishing with sandpaper and ultrasonically cleaned in acetone to remove polish residues. Phase purity of the ceramic sample was checked by XRPD. Density of the sintered ceramic samples of $Sr_{0.7}La_{0.3}Ga_{0.5}In_{0.5}O_{2.65}$, as determined by pycnometry, was 97–98 % relative to X-ray density.

The oxygen diffusion coefficient (D_T) and the surface exchange coefficient (k) for $Sr_{0.7}La_{0.3}Ga_{0.5}In_{0.5}O_{2.65}$ were determined by IEDP technique using SIMS after isotopic exchange of ^{18}O for ^{16}O in the dense ceramic sample prepared by SPS. For isotopic exchange studies the pellet was cut into a rectangular bar (1.0×2.0×4.0 mm). Prior to ^{18}O exchange

annealing, samples were held at 973, 1,073, 1,173, and 1,223 K in air of normal isotopic abundance for a period of time approximately one order of magnitude longer then the tracer annealing time. This was carried out to ensure that the material was in chemical equilibrium at the desired temperature and oxygen partial pressure (in this study all annealings were carried out at a nominal oxygen partial pressure of 0.2 atm). The air was subsequently removed, and labeled oxygen (95 % enriched $^{18}O_2$) was introduced. Annealing times were 62 min at 973 K, 126 min at 1,073 K, 60 min at 1,173 K, and 25 min for 1,223 K. After the isotopic exchange annealing each sample was put into epoxy. The ^{18}O concentration profiles were determined on the polished cross-sections by scanning the surface regions 0.5 mm in length using the TOF-SIMS 5 instrument operated in imaging mode, with a 45° incidence 25 keV Bi^+ primary ion beam.

Netzsch 402C dilatometer operated in air (298–1,173 K, 10 K/min) was used for the thermal expansion coefficient measurements. For this purpose oxide powders of $Sr_2Ga_{1.1}In_{0.9}O_5$ and $Sr_{0.7}La_{0.3}Ga_{0.5}In_{0.5}O_{2.65}$ were pressed into pellets of 8 mm in diameter and 5–5.5 mm in height and annealed at 1,473 K.

AC impedance measurements were used to determine electrical conductivity of dense ceramic sample of $Sr_{0.7}La_{0.3}Ga_{0.5}In_{0.5}O_{2.65}$ prepared by SPS. The sintered sample was a typically made in the shape of a rectangular bar (2.6×7.2×8.7 mm). Pt paste was printed on both sides of the sample and annealed at 1,173 K for 1 h. The impedance spectroscopy measurements were performed on Z-500P (Elins) impedance analyzer in Ar/O_2 mixture ($P_{O_2} = 10^{-4}$–0.21 atm) in the 0.01 Hz to 500 kHz frequency range from 673 to 1,273 K. The oxygen partial pressure was controlled with YSZ oxygen sensor.

Results

Crystal structure of $Sr_2Ga_{1+x}In_{1-x}O_5$, x=0.0–0.2

A majority of the reflections in the XRPD pattern of Sr_2GaInO_5 sample prepared at 1,473 K, 96 h were indexed with a *I*-centered orthorhombic unit cell with a=5.987(2) Å, b=15.234(6) Å, c=5.735(2) Å, therefore indicating the formation of a brownmillerite-type phase. Additional reflections (max ~3 %) observed in the XRPD pattern of Sr_2GaInO_5 were referred to as an admixture of $SrIn_2O_4$. Further re-annealings of this sample did not lead to a decrease of the admixture phase. This indicates that the brownmillerite phase contains slightly less amount of indium in comparison with the nominal composition of the sample. Therefore, the samples with variable amount of indium and gallium ($Sr_2Ga_{1+x}In_{1-x}O_5$, x=0.05–0.2, Δx=0.05) were prepared in the same experimental conditions. The color of the prepared samples was yellowish. Single-phase sample was prepared for $Sr_2Ga_{1.1}In_{0.9}O_5$ (x=0.1). A weak reflection with d=3.07 Å (max ~5 % for x=0.2 sample), which we could not refer to known phases, was observed in the XRPD patterns of the samples with x=0.15 and 0.20. However, unit cell parameters and volume of the brownmillerite phase presented in all studied samples change concomitantly with gallium content. This indicates the existence of a solid solution $Sr_2Ga_{1+x}In_{1-x}O_5$. It should be noted that we were not able to prepare $Sr_2In_2O_5$ and $Sr_2Ga_2O_5$ with brownmillerite structures by heating stoichiometric mixture of $SrCO_3$ and M_2O_3, M=Ga, In in air at 1,473 K, 96 h.

The crystal structure of brownmillerite-like $Sr_2Ga_{1.1}In_{0.9}O_5$ was refined using XRPD data. Since two different structural models are possible for *I*-centered brownmillerite, with ordered

Table 1 Summary of the results of the least-square fits, final atomic coordinates, and displacement parameters for $Sr_2Ga_{1.1}In_{0.9}O_5$

Space group			*Icmm*			
a, Å			5.9694(1)			
b, Å			15.2091(3)			
c, Å			5.7122(1)			
Z			8			
Cell volume, Å^3			518.60(2)			
Density, g/cm^3			5.575			
Radiation			$CuK_{\alpha 1}$, λ=1.54060 Å			
2Θ range; step, deg			7≤2Θ≤100, 0.0081			
Params. refined			35			
χ^2, R_F^2, R_{wp}, R_p			2.48; 0.0504, 0.0605, 0.0458			
Atom	Site	X	y	z	U_{iso}×100/Å^2	Occ.
Sr	8h	0.0247(3)	0.1131(1)	0.5	2.26(7)	1
M	4a	0	0	0	1.9(7)	1
Ga	8i	−0.0770(5)	0.25	−0.025(2)	2.5(2)	0.5[a]
O_1	8g	0.25	−0.0124(6)	0.25	2.6(3)	1
O_2	8h	0.080(2)	0.1505(5)	0	5.6(4)	1
O_3	8i	0.861(3)	0.25	0.641(3)	2.5	0.5[a]

M=0.9In+0.1Ga

[a] Partial occupancies of Ga and O_3 positions resulted from disorder of tetrahedral chains in oxygen-deficient layers of brownmillerite structure

Table 2 Selected interatomic distances (Å) for $Sr_2Ga_{1.1}In_{0.9}O_5$

M-O_1:	(*x*4)	2.0741(8)
M-O_2:	(*x*2)	2.339(8)
Ga-O_2:	(*x*2)	1.786(9)
Ga-O_3:	(*x*2)	1.94(2)
Sr-O_1:	(*x*2)	2.660(5)
	(*x*2)	2.736(3)
Sr-O_2:		2.425(9)
	(*x*2)	2.931(2)
Sr-O_3:	(*x*2)	2.437(9)

M=0.9In+0.1Ga

(S.G. *Ibm2*) or disordered (S.G. *Icmm*) arrangement of tetrahedral chains, they were both tested during the refinement of the crystal structure. Refinement in S.G. *Icmm* resulted in slightly lower *R* values and more reasonable interatomic distances. A summary of the refinement results, final atomic coordinates and displacement parameters for $Sr_2Ga_{1.1}In_{0.9}O_5$ are given in Table 1. Selected interatomic distances are present in Table 2. Observed, calculated XRPD profile intensities and their difference are shown in Fig. 2. Due to the substantial difference in scattering powers for indium and gallium (atomic number 49 and 31, respectively), it was possible to refine relative occupancies of indium and gallium in the octahedral and tetrahedral positions. It was found that the large indium cations are located only in octahedra, while the smaller gallium cations are found in tetrahedra. Bond valence sum calculations performed for the Ga tetrahedral site resulted in quite close to expected one value of 2.85. Since $Sr_2Ga_{1.1}In_{0.9}O_5$ contains an excess of gallium (10 %) in comparison with the amount needed to fully occupy the tetrahedral site, it was located together with indium at the octahedral site.

A study of the high-temperature expansion behavior of $Sr_2Ga_{1.1}In_{0.9}O_5$ in air at 298–1,273 K shows that it expands linearly with a thermal expansion coefficient (TEC) 11.8 ppm K^{-1}. It is close to the TEC=11.4–11.8 ppm K^{-1} reported for Sr and Mg-doped $LaGaO_3$ (LSGM) [12]. No first-order phase transitions were observed in the thermal expansion curve of $Sr_2Ga_{1.1}In_{0.9}O_5$ in the studied temperature range. This is not surprising since a transition to disordered perovskite structure for $Sr_2Ga_{1.1}In_{0.9}O_5$ would involve a step with B-cation disordering, which normally happens at much higher temperatures.

Crystal structure, high-temperature electrical conductivity, and oxygen diffusion in $Sr_{0.7}La_{0.3}Ga_{0.5}In_{0.5}O_{2.65}$

Preparation and crystal structure study of $Sr_{0.7}La_{0.3}Ga_{0.5}In_{0.5}O_{2.65}$

Doping of Sr_2GaInO_5 by La^{3+} according to formula $Sr_{1-y}La_yGa_{0.5}In_{0.5}O_{2.5+x/2}$, y=0.1–0.5, Δy=0.1 resulted in the preparation of nearly single-phase samples only for y=0.3. The color of the y=0.3 sample was light brown. It should be mentioned that several re-grindings and re-heatings of the samples were necessary to achieve equilibrium, e.g., no changes in the corresponding XRPD patterns occurred after further annealing. Samples with y=0.1 and 0.2 contain both brownmillerite and cubic perovskite $(Sr,La)(In,Ga)O_{3-y}$ phase, while y=0.4 and 0.5 a cubic perovskite phase and an increasing amount of $SrLaGa_3O_7$.

A majority of the reflections in the diffraction pattern of the y=0.3 sample were indexed with a cubic perovskite cell with a=4.0291(5) Å (Fig. 3). Additional reflections with intensity <3 % (marked with stars in Fig. 3) were from $SrIn_2O_4$ and unidentified phase(s). No splitting of the perovskite subcell reflections was observed in the XRPD pattern of

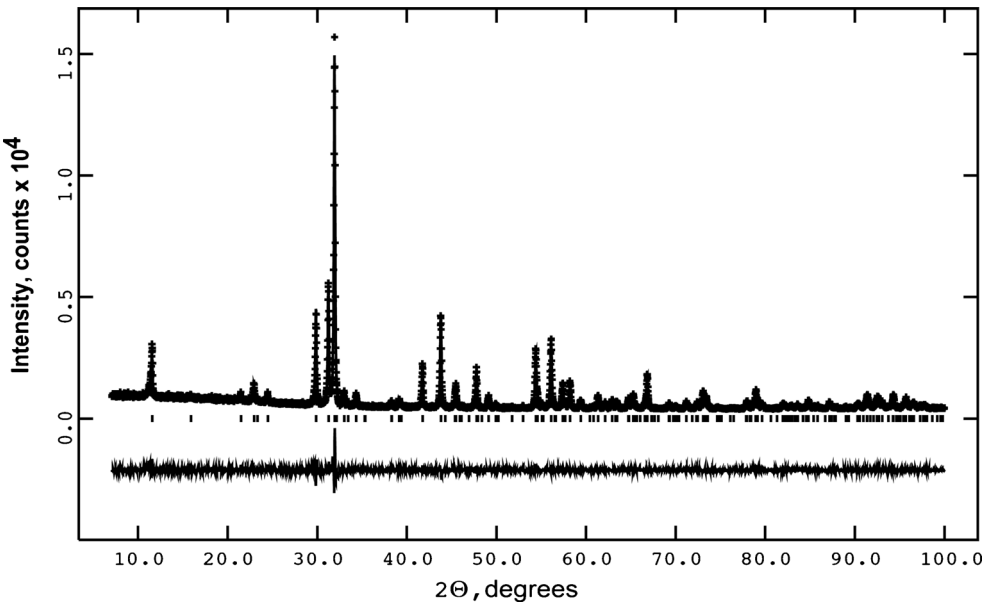

Fig. 2 Observed, calculated XRPD profiles of $Sr_2Ga_{1.1}In_{0.9}O_5$ and difference between them

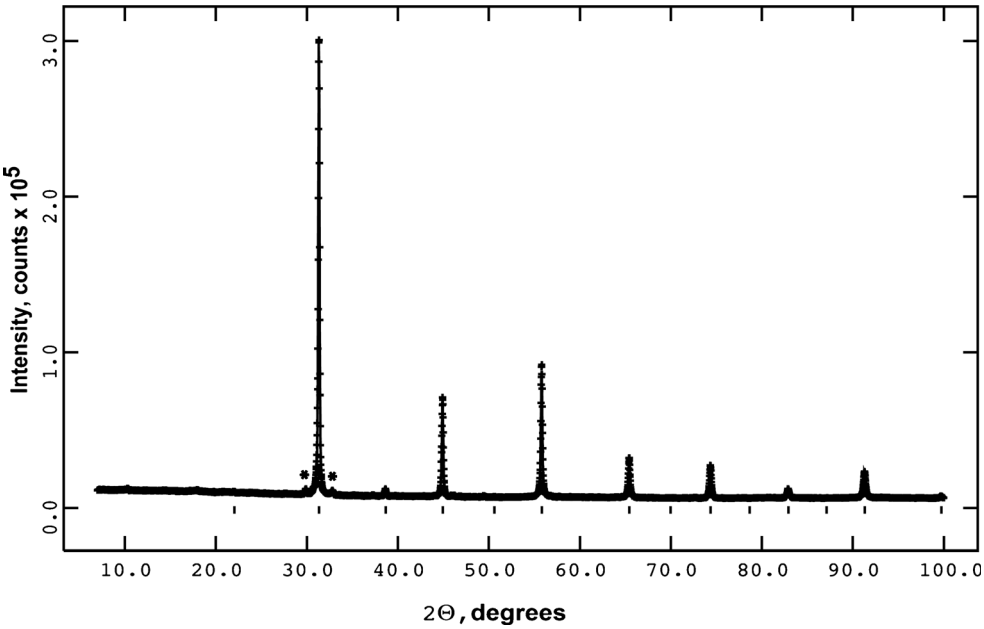

Fig. 3 XRPD pattern for $Sr_{0.7}La_{0.3}Ga_{0.5}In_{0.5}O_{2.65}$. Reflections from admixture phases are marked with *stars*

$Sr_{0.7}La_{0.3}Ga_{0.5}In_{0.5}O_{2.65}$ indicating true cubic symmetry and complete disorder of cations and oxygen vacancies in the crystal structure. This result was confirmed by ED study, which showed no additional superstructure reflections on selected-area ED (SAED) patterns of $Sr_{0.7}La_{0.3}Ga_{0.5}In_{0.5}O_{2.65}$ (Fig. 4).

Measurements of the thermal expansion behavior of $Sr_{0.7}La_{0.3}Ga_{0.5}In_{0.5}O_{2.65}$ at 298–1,173 K in air revealed linear expansion with TEC = 12.6 ppm K^{-1}, higher in comparison with brownmillerite-like $Sr_2Ga_{1.1}In_{0.9}O_5$.

Oxygen diffusion in $Sr_{0.7}La_{0.3}Ga_{0.5}In_{0.5}O_{2.65}$ studied by SIMS

The oxygen diffusion in $Sr_{0.7}La_{0.3}Ga_{0.5}In_{0.5}O_{2.65}$ was studied by SIMS and as an example, the ^{18}O isotopic concentration depth profile of $Sr_{0.7}La_{0.3}Ga_{0.5}In_{0.5}O_{2.65}$ annealed at 1,073 K is given in Fig. 5. The oxygen tracer diffusion (D_T) and surface exchange (k) coefficients were determined by non-linear least squares regression based on fitting of the diffusion profiles using the Crank relation, solution of the Fick's second law of the diffusion, similar to the procedure described in references [13, 14]. Calculated values of D_T and k at various temperatures are given in Table 3. Dependences of bulk oxygen tracer diffusion and surface exchange coefficients on reverse temperature are given in Fig. 6. They can be perfectly fitted by Arrhenius law with activation energies (E_a) 1.4(1) eV and 1.1(1) eV for the oxygen tracer diffusion and the surface exchange coefficients, respectively. The values of the oxide-ion conductivity (σ_O) presented in Table 3 were calculated from D_T using the Nernst–Einstein equation

$$\sigma_O = \frac{4N \cdot e^2 \cdot D_{self}}{k_B \cdot T},$$

where N is the concentration of oxygen vacancies in unit cell volume, e is the electron charge, D_{self} is oxygen self-diffusion coefficient which was considered to be equal to D_T oxygen tracer diffusion coefficient, k_B is the Boltzmann constant, and T is the absolute temperature.

High-temperature electrical conductivity of $Sr_{0.7}La_{0.3}Ga_{0.5}In_{0.5}O_{2.65}$

AC impedance spectra at T = 1,083–1,213 K and at variable oxygen partial pressure (P_{O_2}) at 1,213 K are shown at Fig. 7a

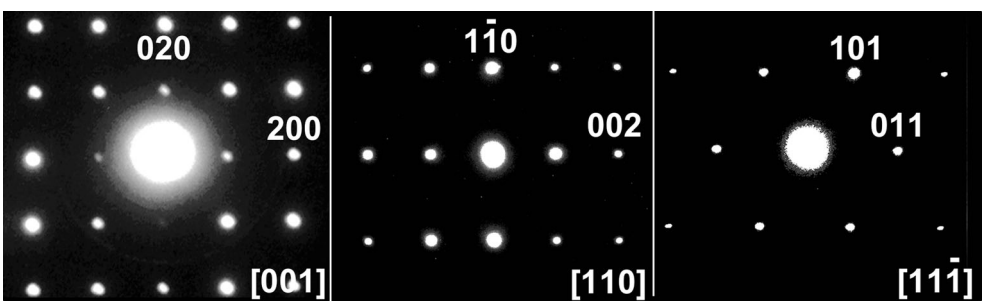

Fig. 4 SAED pattern of the cubic perovskite $Sr_{0.7}La_{0.3}Ga_{0.5}In_{0.5}O_{2.65}$ viewed along [001], [110], and [11-1]

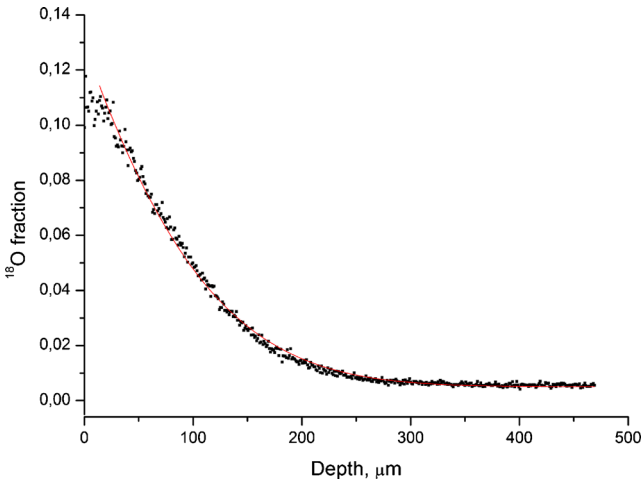

Fig. 5 ^{18}O penetration profile determined for $Sr_{0.7}La_{0.3}Ga_{0.5}In_{0.5}O_{2.65}$ at 1,223 K. The *points* refer to experimental data, and the curve for the fitting results

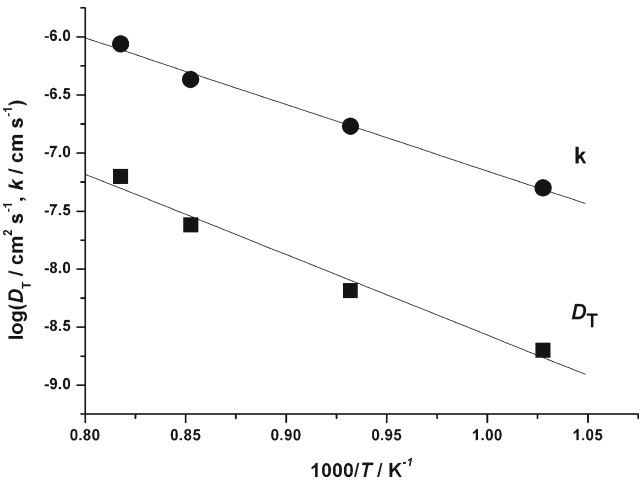

Fig. 6 Bulk oxygen tracer diffusion (D_T) and surface exchange (k) coefficients obtained for $Sr_{0.7}La_{0.3}Ga_{0.5}In_{0.5}O_{2.65}$ as a function of the inverse temperature. *Circles* refer to surface exchange, *squares* to oxygen tracer diffusion coefficients

and b, respectively. The impedance spectra of Pt/$Sr_{0.7}La_{0.5}Ga_{0.3}In_{0.5}O_{2.65}$/Pt system are composed of one depressed semicircular arc and can successfully be described by the equivalent circuit shown in the inset of Fig. 7b. It should be noted that it is not possible to separate bulk and grain boundary resistances for the whole studied temperature range. The equivalent circuit is a series connection of resistance (R_1) and (R_2−CPE) element. The resistance R_1 does not depend on P_{O_2}, while R_2 increases significantly with the decreasing of P_{O_2}. One can conclude that resistance R_1 corresponds to the total resistance of the sample and, therefore, that the semicircular arc and the difference (R_2−R_1) correspond to the electrode impedance and electrode polarization resistance, respectively.

The temperature dependence of the total conductivity of $Sr_{0.7}La_{0.3}Ga_{0.5}In_{0.5}O_{2.65}$ at variable oxygen pressure is given in Fig. 8a. The values of the conductivity are nearly independent on oxygen partial pressure as can be observed from isothermal logσ versus log P_{O_2} curves shown in Fig. 8b. The dependence of logσ versus (1/T), shown in Fig. 8a, can be fitted very satisfactorily by Arrhenius law in the whole studied temperature range with activation energy (E_a) 1.08±0.01 eV.

The close to independent total conductivity of $Sr_{0.7}La_{0.3}Ga_{0.5}In_{0.5}O_{2.65}$ with oxygen partial pressure indicates that oxide-ion conductivity pre-dominate at the studied experimental conditions. However, one can notice a very weak oxygen partial pressure dependence of the conductivity, reflected as a slight increase of the log σ with increasing log P_{O_2} at low temperatures (Fig. 8b). This can be explained by the creation of holes ($h^{\bullet}$) according to the following mechanism:

$$\frac{1}{2}O_2(g) + V_O^{\bullet\bullet} \rightarrow O_O^x + 2h^{\bullet} \qquad (1,)$$

where $V_O^{\bullet\bullet}$ is an oxygen vacancy, O_O^x is an oxygen atom at regular position according to Kröger–Vink notations. Therefore, the total conductivity (σ_{tot}) of $Sr_{0.7}La_{0.3}Ga_{0.5}In_{0.5}O_{2.65}$

Table 3 Values of D_T, k, and σ_O for $Sr_{0.7}La_{0.3}Ga_{0.5}In_{0.5}O_{2.65}$ at various temperatures

T, K	D_T, cm^2/s	k, cm/s	σ_O, S/cm[a]
973	2.0×10^{-9}	5.0×10^{-8}	8.18×10^{-5}
1,073	6.5×10^{-9}	1.7×10^{-7}	2.41×10^{-4}
1,173	2.4×10^{-8}	4.3×10^{-7}	8.14×10^{-4}
1,223	6.3×10^{-8}	8.7×10^{-7}	2.05×10^{-3}

[a] Calculated from D_T using the Nernst–Einstein equation

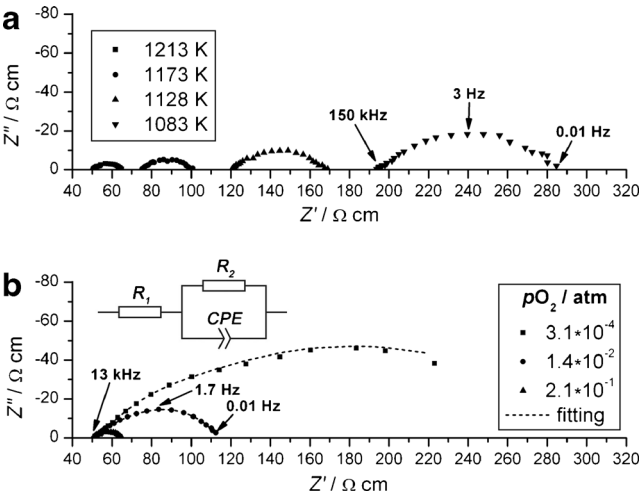

Fig. 7 AC impedance data for Pt/$Sr_{0.7}La_{0.3}Ga_{0.5}In_{0.5}O_{2.65}$/Pt system at variable temperature (**a**) and at T=1,213 K at variable oxygen pressure (**b**). The equivalent circuit used to interpret the data is shown in the *inset*. Experimental points are shown by *symbols* while *dashed lines* correspond to the fitted by using equivalent circuit

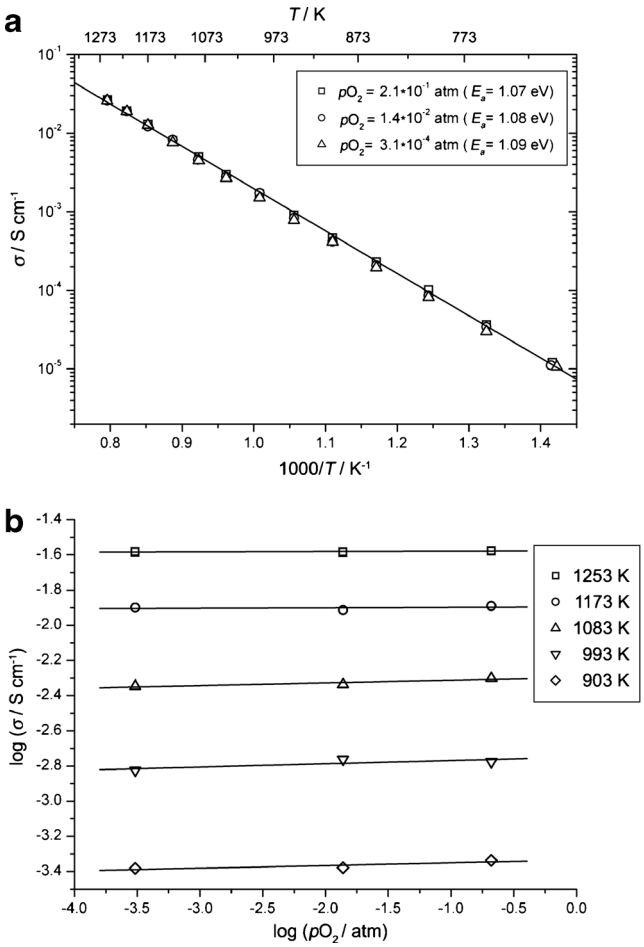

Fig. 8 **a** Arrhenius plot of the total conductivity versus the inverse of temperature of $Sr_{0.7}La_{0.3}Ga_{0.5}In_{0.5}O_{2.65}$ at variable oxygen pressure. **b** Dependence of the total conductivity of $Sr_{0.7}La_{0.3}Ga_{0.5}In_{0.5}O_{2.65}$ versus oxygen pressure at fixed temperature

can be expressed as a sum of oxide-ion (σo) and hole ($\sigma_h\cdot$) conductivities and expressed by the following Eq. [15]:

$$\sigma_{tot} = \sigma_O + \sigma_h\cdot = a + b\cdot p_{O_2}^{1/4} \quad (2.)$$

Since only $\sigma_h\cdot$ shows a P_{O_2} dependence, Eq. 2 allows a separation values of σ_O and $\sigma_h\cdot$ at a fixed temperature. The temperature dependences of the total, hole, and oxide-ion conductivities for $Sr_{0.7}La_{0.3}Ga_{0.5}In_{0.5}O_{2.65}$ are shown in Fig. 9. Below 1,073 K, the temperature dependences of the logarithm of the hole and oxide-ion conductivities versus ($1/T$) are linear with activation energies 0.96 and 1.10 eV, respectively. It should be noted that the value of the activation energy for oxide-ion conductivity is close to that one obtained by SIMS (1.4(1) eV). For $T>1{,}073$ K the oxide-ion conductivity continues to increase, while the *p*-type conductivity saturates. This leads to an increased transport number for the oxide-ion conductivity (t_O) to values close to 1 in the high-temperature region (Fig. 10). The values of the oxide-ion conductivity of

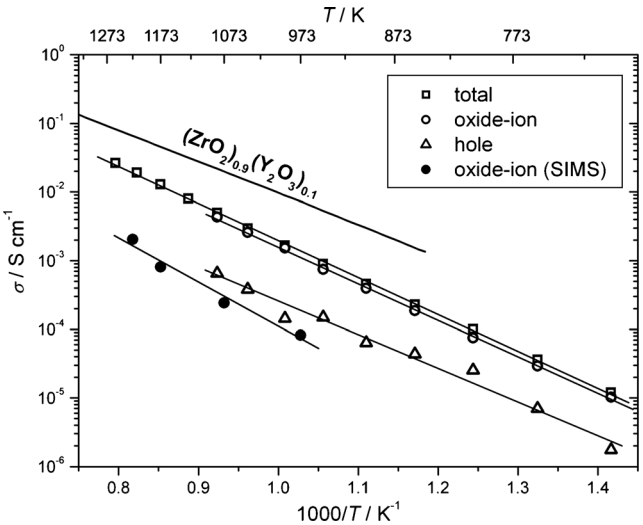

Fig. 9 Temperature dependence of the total, oxide-ion, and hole conductivities for $Sr_{0.7}La_{0.3}Ga_{0.5}In_{0.5}O_{2.65}$. Values for the conductivity of $(ZrO_2)_{0.9}(Y_2O_3)_{0.1}$ from reference [16] are given for the comparison. Values of oxide-ion conductivity of $Sr_{0.7}La_{0.3}Ga_{0.5}In_{0.5}O_{2.65}$ calculated from oxygen tracer diffusion coefficients determined by SIMS using Nernst–Einstein equation are also present

$Sr_{0.7}La_{0.3}Ga_{0.5}In_{0.5}O_{2.65}$ as calculated from oxygen tracer diffusion coefficients D_T using Nernst–Einstein equation, see Table 3, are substantially lower in comparison with those one determined from AC impedance data (Fig. 9). Disagreement between values of oxide-ion conductivity obtained by different techniques is also reported in the literature, see, for example, reference [17].

Discussion

In spite of the thermodynamic instability of brownmillerite-type $Sr_2In_2O_5$, this structure can be stabilized for the complex oxides $Sr_2Ga_{1+x}In_{1-x}O_5$ with x close to 0 and with the Ga^{3+}

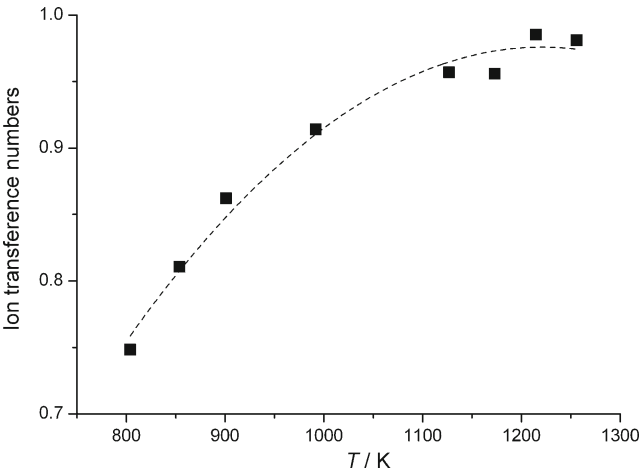

Fig. 10 Temperature dependence of oxide-ion transport number (t_O) for $Sr_{0.7}La_{0.3}Ga_{0.5}In_{0.5}O_{2.65}$. *Dashed line* is to guide the eyes only

and In^{3+} cations ordered in the tetrahedral and octahedral positions, respectively. The most plausible explanation for the instability of $Sr_2In_2O_5$ compared to $Ba_2In_2O_5$ is the misfit between the long In-O interatomic distances ($d(In\text{-}O)_{average}$=2.01 Å), due to the large ionic radius of In^{3+}, in the InO_4 tetrahedra, and the short Sr-O distances ($d(Sr\text{-}O)_{average}$=2.70 Å) [8] for this structure type. The mismatch is obviously smaller in $Ba_2In_2O_5$, where the corresponding distances are $d(In\text{-}O)_{average}$=2.05 Å and $d(Ba\text{-}O)_{average}$=2.83 Å, respectively [18]. The complete substitution of In^{3+} in the tetrahedra by the smaller Ga^{3+}, as in $Sr_2Ga_{1+x}In_{1-x}O_5$, resolves this problem making brownmillerite structure stable. A specific feature of the brownmillerite structure (Fig. 1) is the presence of distorted MO_6 octahedra with substantially elongated axial M-O bonds. The appearance of GaO_4 tetrahedra resulted in an increasing axial distortion of the InO_6 octahedra, which happens due to the necessity to compensate shrinking of the tetrahedra because of the much smaller size of Ga^{3+} cation in comparison with In^{3+} one. The axial distortion of InO_6 in $Sr_2Ga_{1.1}In_{0.9}O_5$, defined as the difference between the axial and equatorial bond lengths normalized by their average is 0.12. This value is substantially larger in comparison with both $Ba_2In_2O_5$ (0.08) and $Sr_2In_2O_5$ (0.06).

One of the ways to create disorder in the oxygen sublattice in brownmillerite-like compounds and thereby stabilizing a cubic perovskite structure is a partial heterovalent substitution of cations resulting in an increase of the oxygen content. In the case of brownmillerite-type $Sr_2Ga_{1+x}In_{1-x}O_5$ it was achieved by partial replacement of Sr^{2+} by La^{3+} according to chemical formula $Sr_{1-y}La_yGa_{0.5}In_{0.5}O_{2.5+x/2}$. Surprisingly, such compound was only obtained for y=0.3 and with no or very narrow homogeneity range. As expected, the introduction of additional oxygen atoms in tetrahedral layers of brownmillerite structure does result in the formation of the cubic perovskite $Sr_{0.7}La_{0.3}Ga_{0.5}In_{0.5}O_{2.65}$ with complete disorder in both anion and cation sublattices. Obtained by SIMS values of the oxygen trace diffusion coefficient D_T at 1,073 K and $E_{a(D)}$ for $Sr_{0.7}La_{0.3}Ga_{0.5}In_{0.5}O_{2.65}$ (6.5×10^{-9} cm^2/s and 1.4(1) eV) are close to those ones reported for Ca-doped ZrO_2 ($Zr_{0.858}Ca_{0.142}O_{1.858}$)—$7.54\times10^{-9}$ cm^2/s and 1.53 eV [19]. However, D_T values for typical SOFC electrolytes like YSZ ($Zr_{0.81}Y_{0.19}O_{1.905}$) [20], $(Y_2O_3)_2(Sc_2O_3)_9(ZrO_2)_{89}$ [17], and GDC ($Ce_{0.9}Gd_{0.1}O_{1.95}$) [20] are by one order of magnitude higher—6.2×10^{-8}, 1.84×10^{-7}, and 2.7×10^{-8} cm^2/s (1,073 K), respectively. Moreover, LSGM ($La_{0.8}Sr_{0.2}Ga_{0.8}Mg_{0.2}O_{2.8}$) shows an even higher value of $D_T=4.13\times10^{-7}$ cm^2/s (1,073 K) [21]. The origin of the lower oxide-ion conductivity in $Sr_{0.7}La_{0.3}Ga_{0.5}In_{0.5}O_{2.65}$ seems to be the very high preference of Ga^{3+} for the tetrahedral environment. One can speculate about the localization of oxygen vacancies near Ga^{3+} resulting in formation of GaO_4 tetrahedra at the local level in $Sr_{0.7}La_{0.3}Ga_{0.5}In_{0.5}O_{2.65}$. Such a local ordering of oxygen vacancies was revealed by an EXAFS study of $Ba_2In_{2-x}GaxO_5$ [6]. Therefore, the increased activation energy of oxide-ion diffusion from InO_6 octahedra to GaO_4 tetrahedra may be expected. This conclusion can be supported by potential energy surface study in Ga and Sr doped $Ba_2In_2O_5$ [22]. In $Sr_{0.7}La_{0.3}Ga_{0.5}In_{0.5}O_{2.65}$ the situation is even more complicated due to low stability of In^{3+} with CN<6 in complex oxides with small A-cations like Sr^{2+}. It should be also noted that $Ba_{0.3}Sr_{0.2}La_{0.5}InO_{2.75}$ exhibits much higher value of oxygen conductivity in contrast to $Sr_{0.7}La_{0.3}Ga_{0.5}In_{0.5}O_{2.65}$: 0.12 S/cm [4] and 5.0×10^{-3} S/cm at 1,073 K, respectively. The possible explanation of this difference can be larger bottleneck space for oxide-ion diffusion in the case of Ba-contained phase.

It should be noted that in comparison with barium and indium mixed oxides like $Ba_2In_2O_5$ [3] or $Ba_4In_6O_{13}$ [23], $Sr_{0.7}La_{0.3}Ga_{0.5}In_{0.5}O_{2.65}$ does not show significant p-type conductivity. A similar result was obtained in reference [6], where $Ba_2In_{1.5}Ga_{0.5}O_5$ was found to exhibit nearly pure oxide-ion conductivity in contrast to what is observed for un-doped $Ba_2In_2O_5$. The reason can be the presence of randomly distributed Ga^{3+} in the perovskite structure. As a result the oxide-ion transport number (Fig. 10) approaches 1 in the high-temperature region.

Conclusions

$Sr_2Ga_{1+x}In_{1-x}O_5$ system shows an example of the stabilization of the brownmillerite structure by B-cation size effect, due partial replacement of large In^{3+} cations by smaller Ga^{3+} ones. A study of the crystal structure of $Sr_2Ga_{1.1}In_{0.9}O_5$ reveals ordering of Ga^{3+} and In^{3+} cations over tetrahedral and octahedral positions, respectively. A partial replacement of Sr^{2+} by La^{3+} according to the formula $Sr_{1-y}La_yGa_{0.5}In_{0.5}O_{2.5+x/2}$ leads to the formation of cubic perovskite for y=0.3. Study of high-temperature electrical transport of $Sr_{0.7}La_{0.3}Ga_{0.5}In_{0.5}O_{2.65}$ reveals nearly pure oxide-ion conductivity at high temperature. However, the value of oxide-ion conductivity is about two orders of magnitude lower as compared to $Ba_{0.3}Sr_{0.2}La_{0.5}InO_{2.75}$ and LSGM. This is most likely due to higher oxygen vacancy concentration in $Sr_{0.7}La_{0.3}Ga_{0.5}In_{0.5}O_{2.65}$ and their localization near Ga^{3+} cations resulting in formation of stable GaO_4 tetrahedra.

Acknowledgments This work was partially supported by Ministry of Science and Education of Russian Federation (state contract 14.740.12.1358), Russian Foundation for Basic Research (grant no. 11-08-01159a and 11-03-01225), and MSU-development Program up to 2020. This work is financially supported by the Swedish Research Council (VR) and the Baltic Sea/Visby program from the Swedish Institute. The electron microscopy facility was supported by Knut and Alice Wallenberg Foundation.

References

1. Steele BCH (2001) J Mater Sci 36:1053–1068
2. Huang K, Tichy RS, Goodenough JB (1998) J Am Ceram Soc 81:2565–2575

3. Goodenough J, Ruez-Diaz J, Zhen Y (1990) Solid State Ionics 44:21–31
4. Kakinuma K, Yamamura H, Haneda H, Atake T (2002) Solid State Ionics 154–155:571–576
5. Kakinuma K, Arisaka T, Yamamura H, Atake T (2004) Solid State Ionics 175:139–143
6. Yao T, Uchimoto Y, Kinuhata M, Inagaki T, Yoshida H (2000) Solid State Ionics 132:189–198
7. Hashimoto T, Yoshinaga M, Nakano K, Omoto K, Sugimoto T, Tanaka M, Yashima MJ (2009) Ceram Soc Jpn 117:56–59
8. von Schenk R, Mueller-Buschbaum H (1973) Z Anorg Allg Chem 395:280–286
9. Chernov SV, Dobrovolsky YA, Istomin SY, Antipov EV, Grins J, Svensson G, Tarakina NV, Abakumov AM, Van Tendeloo G, Erikson SG, Rahman SMH (2012) Inorg Chem 51:1094–1103
10. Shannon RD (1976) Acta Crystallogr A32:751–767
11. Larson AC, Von Dreele RB (2000) General structure analysis system (GSAS). Los Alamos National Laboratory Report LA-UR-86-748; Toby BH (2001) EXPGUI, a graphical user interface for GSAS. J Appl Cryst 34:210–213
12. Ullmann H, Trofimenko N, Tietz F, Stoever D, Ahmad-Khanlou A (2000) Solid State Ionics 138:79–90
13. Boehm E, Bassat J-M, Steil MC, Dordor P, Mauvy F, Grenier J-C (2003) Solid State Sci 5:973–981
14. Kilner A, De Souza RA, Fullarton IC (1996) Solid State Ionics 86–88: 703–709
15. Song S-J, Wachsman ED, Doris SE, Balachandran UJ (2003) Electrochem Soc 150:A790–A795
16. Minh NQ, Takashi T (1995) Science and technology of ceramic fuel cells. Elsevier, Amsterdam
17. Raj ES, Atkinson A, Kilner JA (2009) Solid State Ionics 180: 952–955
18. Berastegui P, Hull S, Garcia-Garcia FJ, Erikson S-GJ (2002) Solid State Chem 164:119–130
19. Simpson LA, Carter REJ (1966) Am Ceram Soc 49:139–144
20. Manning PS, Sirman JD, Kilner JA (1997) Solid State Ionics 93: 125–132
21. Ishihara T, Kilner JA, Honda M, Sakai N, Yokokawa H, Takita Y (1998) Solid State Ionics 113–115:593–600
22. Mohn CE, Allan NL, Stølen S (2006) Solid State Ionics 177: 223–228
23. Abakumov AM, Rossell MD, Gutnikova OY, Drozhzhin OA, Leonova LS, Dobrovolsky YA, Istomin SY, Van Tendeloo G, Antipov EV (2008) Chem Mater 20:4457–4467